J. Adv. Appl. NanoBio Tech.
ISSN: 2710-4001

Journal web link:
http://www.AANBT.dormaj.com
https://doi.org/10.47277/AANBT/2(4)23

A comparative study on the clays incorporated with acrylamide-based hydrogels

Farzaneh Sabbagh [*1], Khadijeh Kiarostami[1], Nadia Mahmoudi Khatir[2]

1Department of Plant Sciences, Faculty of Biological Science, Alzahra University, 1993891176, Tehran, Iran
2Department of Biotechnology, Faculty of Biological Science, Alzahra University, 1993891176, Tehran, Iran

Received:15/07/2021 Accepted:28/07/2021 Published: 20/12/2021

Abstract

In the current study to increase the release ability of acrylamide-based hydrogels, modified acrylamide-based hydrogel nanocomposites were synthesized and Montmorillonite, Kaolinite, and Illite were added to the matrix. The characterization of the clays was carried out using EDX and XRD, whereas the characterization of the clay-hydrogels was carried out with Fourier transform infrared spectroscopy (FTIR), Field Emission Scanning Electron Microscope (FESEM), swelling ratio, and rheology measurements. EDX of clays showed that the highest amount of Al (17.18±0.12%) is for Kaolinite and the highest amount of Si (20.94±0.85%) and Fe (8.53±0.17%) belongs to Illite. The highest amount of C (6.97±1.54%) is for Montmorillonite. The swelling of Montmorillonite/Aam hydrogels including was found to be higher than other types of hydrogels used in this study. The shifting of the bonds in FTIR and FESEM images of composites showed that the clays are well-incorporated to the polymer and the shape of the composites in the FESEM images indicates the effect of clays on the structure of polymers. The highest swelling ratio was attributed to Montmorillonite/Aam composite. The frequency sweep test showed that the G' and G" value of the Illite/Aam G' (1260±36.5 Pa) and (198.5±6.6 Pa) was higher than the other mixtures.

Keywords: *Composite Hydrogel, Clay-polymer Nanocomposite, Acrylamide, Swelling Behavior, Drug Delivery Carriers, Montmorillonite*

[1] **Corresponding author:** Farzaneh Sabbagh, Department of Plant Sciences, Faculty of Biological Science, Alzahra University, 1993891176, Tehran, Iran
f.sabagh@alzahra.ac.ir

1 Introduction

Hydrogels are intelligent three-dimensional polymer networks that contain a large amount of water and displaying changes in volume responding to small changes, known as soft and wet matter, the same as biological soft tissues [1, 2]. Polymer/clay nanocomposites also have some interesting advantages when compared to pure polymers, such as enhanced mechanical [3]. These benefits along with the good intercalation capacity offered by clay mineral particles have been widely exploited to develop new controlled release systems. Polyacrylamide has been chosen as a polymer because its hydrogels are pH-sensitive [4]. Polymer/clay nanocomposites are a class of hybrid systems in which clay/organo-clay nanoparticles are dispersed in a polymer matrix. The application of clays in the hydrogels provides many advantages to the targeted delivery, thereby improving the firmness and bioavailability of therapeutic agents against degradation and the extending impact of the drug in the targeted tissue [5]. As clays have unique physicochemical characteristics and high specific surface area, they can be employed widely for various applications [6]. These materials can absorb huge amounts of water and can swell due to the presence of various hydrophilic groups such as –OH, –COOH, –NH2, –CONH2, and –SO3H in their structures [7] and can form a linked network of hydrophilic polymers [8]. Some new functional groups can be added to them to modify their structure or can be prepared as composites to enhance the chemical/physical characteristics[9]. Metal oxides such as MgO are interesting due to their requirement as essential minerals for the health and also their stability under strict conditions[10]. The nano- and micro-sized MgO particles have attracted attention because of their numerous biomedical applications. Clays are the common ingredients present in pharmaceutical products both as active substances and excipients. Moreover, clay minerals play a crucial role in modulating drug delivery and are the first step to provide therapeutically effective systems. The investigation of clay–drug interaction and release mechanisms is essential in formulating clay-based drug delivery systems [11]. In this work, we use exfoliated sodium Montmorillonite as noncovalent cross-linkers for a novel synthesis of tough hydrogels. Montmorillonite is a layered silicate clay constituted by two tetrahedral silica sheets sandwiching an octahedral sheet formed from cations such as Al3+ or Mg2+, with a formula of [(Al, Mg)4Si8O20(OH)4] Na0.66 [12]. Illite content in slime water can be up to 20% of all clay particles and it seriously affects the sedimentation of the slime water [13]. Illite, as one of the abundant natural minerals, is a 2:1 sandwich of silica tetrahedral - alumina octahedral - silica tetrahedral layers with rich hydrophilic aluminum hydroxyl [14, 15]. Its particles are typically 0.1–0.4 μm wide and only a few 100 Å thick. Their length varies enormously but can be tens of micrometers. The K, Mg, or Ca interlayer cations avoid the entrance of H2O into the structure. Therefore, the Illite clays are non-developing clays. Among clay minerals, Kaolinite is one of the most common 1:1 type layered silicate, which consists of one tetrahedral (Si-O) sheet and one octahedral (Al-OH) sheet and is mainly used in ceramics, pottery, coatings, and filler [16]. They are hydrous aluminum silicates and consist of the principal components of kaolin. Kaolinite is the purest clay, and it varies slightly in composition.

This research is aimed to synthesize and characterize the acrylamide/clay structure of Montmorillonite, Illite, and Kaolinite to compare the morphological, and structural differences of the nanocomposites. The main purpose of this idea is to evaluate the best clay among montmorillonite, Kaolinite, and Illite for further studies about drug delivery.

2. Experimental

2.1 Materials

Acrylamide, N, N'-methylene bisacrylamide (MBA), N, N, N', N' -tetramethyl ethylene diamine (TEMED), ammonium persulfate (APS), Illite, Kaolinite, Montmorillonite were procured from Sigma Aldrich Malaysia. All the chemicals were of the analytical grade. Distilled water was used in all the steps of the experiments.

2.2 EDX of Clays

In this study, EDX spectrometer Model JEOL-Jsm-5910; Japan was used. The EDX maps were acquired with a Bruker EDX system for elemental analysis. A 10 mm distance with an accelerating voltage of 15 kV was performed[17].

2.3 XRD of Clays

The powdered clays sample purity was checked by using X-ray diffraction. Its chemical composition was determined using elemental analysis (carried out using fluorescence), which resulted in the unit cell formula. X-ray diffraction quantities of clays were carried out at room temperature, expending using Siemens Diffraktometer D5000 X-ray diffractometer with Cu Kα at 40keV and 40mA with a step length of 0.05o and step time of 1s. The diffraction angle (2θ) was between 20 and 80 [18].

2.4 Preparation of Acrylamide Hydrogels

Hydrogel synthesis was carried out as follows: 0.4 g of acrylamide and 0.01 g clay (Montmorillonite, Illite, or Kaolinite) was dissolved in 20ml of distillate water at 80ºC and 0.04 g of N, N'-methylene bisacrylamide (MBA) as cross-linker was then added to the solution. The hot mixture was kept under gentle stirring for approximately 15 minutes to form a homogenous, clear, and viscous solution with the absence of bubbles. Finally, 0.01 g of N, N, N', N'-tetramethyl ethylenediamine (TEMED) and 0.01 g of ammonium persulfate (APS) as an initiator was added to the solution at the same temperature and stirred immediately to prevent the changing of the solution to gel after a few seconds [19].

2.5 FTIR analysis of hydrogel

A Fourier transform infrared spectroscopy (FTIR) (Nicolet 670 FTIR, USA) was used to analyze the samples. The amount of 4 mg of dried hydrogels was prepared and mixed with KBr (1:10). The pressure of the hydraulic press was 500 kg/cm2. 1.0 cm-1 interval for 16 scans was applied. The resolution of 4 in the region 370 and 4000 cm-1[19].

2.6 Hydrogel nano composites microstructure

Using a gold sputter coater Bio-Rad Polaran Division (E6700, USA), the samples were coated under vacuum. To keep the pores of hydrogels, the first samples were freeze-dried and were

left in liquid nitrogen as intact for imaging. Hydrogels were studied at the voltage of 10 kV and magnification of 5000× and 1000× [20].

2.7 Swelling studies

The swelling ratio of hydrogels was investigated by immersion of samples in distilled water. Periodically, the weight of the swelling ratio was measured and then was calculated by the following equation:

$$\text{Swelling ratio (\%)} = \left[\frac{Wt-W0}{W0}\right] \times 100 \quad \text{(Equation 1)}$$

where Wt is the swollen gels' weight at time t and W0 is the original weight of sample.

2.8 Rheological measurement

The rheological experiments of the hydrogels were run by Physica MCR301 controlled strain /stress rheometer (Anton Paar GmbH, Germany) which a cone plate system (0.206 mm gap, 50 mm diameter, and 4° angle) was attached. After putting on the rheometer plate, they were allowed to relax for 10 minutes before the measurements. To keep and control the temperature of the bottom plate, the samples were covered by a protective hood. A Peltier system (Viscotherm VT2, Phar Physica) was used to preserve temperature regularity in active mode during the test [21].

2.8.1 Frequency sweep analysis

This test was conducted at a constant temperature (20 ℃), constant stress in the LVE region (0.1 Pa), and frequency range of 0.01-10 Hz to evaluate the viscoelastic properties of samples. To avoid evaporation of sample during measurements, in the dynamic test, a thin layer of silicone oil coated the rim of the sample[21].

Statistical analysis

At least three replications were performed for all of the experiments. A completely randomized design was applied for statistical analysis. All formulations were expressed as mean ± standard deviation. To define a statistically significant difference between samples, a one-way analysis of variance (ANOVA) with the post "Tukey's post hoc test" for multiple comparisons was conducted by employing SPSS software (SPSS, version 20). A p-value of less than 0.05 was considered statistically significant.

3. Results and Discussion

3.1 Synthesis of nanocomposite

Polyacrylamide/clay nanocomposite was synthesized by the reaction between the monomer (acrylamide) and three different clays. The clays were linked due to the hydrogen bonding between amide & hydroxyl groups present on graft copolymer.

3.2 XRD of clays

To investigate the composition of clays, an XRD test was performed in **Figure 1**. The structure of three clays as well as Illite, Kaolinite, and Montmorillonite was estimated with x-ray diffraction (XRD).

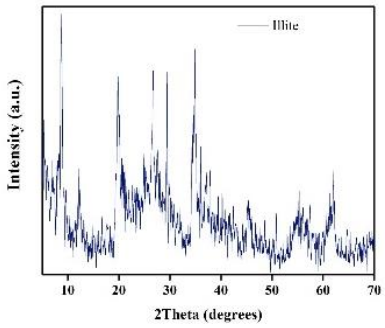

(a)

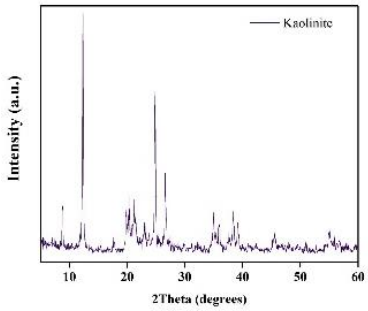

(b)

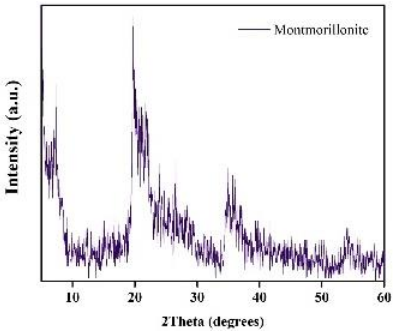

(c)

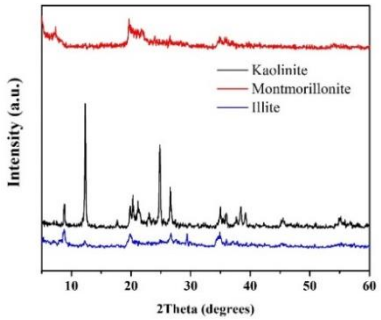

(d)

Figure 1. The XRD pattern of a) Illite, b) Kaolinite, c) Montmorillonite, and d) a comparative graph of the clays

To consider the crystal structure of hydrogels, an X-ray diffraction technique was applied. In-phase radiation can be realized as a peak in the XRD pattern. According to Bragg's law (nk=2d. sinh), X-ray diffraction analysis forms the basis for the identification of microfabric of clay minerals [22]. The wavelength of X-rays is signed with k, and the whole number for the order of reflection is signed by n. Brindley used an X-ray powder camera to the measure structure of clays, and shales[23]. Ong and Hewat reported that the structure of Kaolinite clay is triclinic [24]. It consists of SiO2 (silica) tetrahedral sheets bonded to sheets of Al2O3 alumina octahedral[25]. Natural montmorillonites usually present isomorphic substitutions in both tetrahedral and octahedral layers [26]. The weak intensity and broad peak profile of the montmorillonite reflection are likely a result of internal disorder. The XRD pattern of the Illite presented it contained Illite clay mineral as the major phase, with quartz, microcline , and kaolinite present as minor phases [27, 28]. **Table 1** shows some higher intensity of the reflection of the material at various 2θ degrees.

Table 1. Some higher intensity of Illite, Kaolinite and Montmorillonite reflection at various 2θ degrees

Material	2θ degrees
Illite	5.28, 8.8, 19.85, 29.4, 55.25,61.95
Kaolinite	8.8, 12.3, 24.85, 35, 38.4,45.5
Montmorillonite	7.35, 19.65, 21.8. 26.45,35, 36

3.3 EDX

An energy-dispersive X-ray analyzer (EDX) was used to determine the chemical composition of Illite, Kaolinite, and Montmorillonite. The quantitative EDX analysis (**Table 2**) suggests Si and Al as dominant in the Illite and Kaolinite. **Figure 2** presents the chemical structure of clays which indicates that Si (20.94±0.85%) in Illite and Al (17.18±0.12%) in Kaolinite is the main components of the Kaolinite and Illite, however, C (6.97±1.54%) in Montmorillonite and Fe (8.53±0.17%) in Illite which are common are found in smaller quantities. The EDX analysis showed the presence of a very high amount of Al, Si in this fraction. Si and Al are the main components of ingredients, with C and Fe. Fe found in small quantities confirms the presence of Illite as indicated by XRD.

Table 2. The EDX of Illite, Kaolinite and Montmorillonite

Clay	Si (Weight%)	Al (Weight%)	C (Weight%)	Fe (Weight%)
Montmorillonite	9.97±0.12	5.96±0.16	6.97±1.54	0.62±0.5
Illite	20.94±0.85	10.24±0.38	3.30±0.30	8.53±0.17
Kaolinite	19.90±0.60	17.18±0.12	6.54±0.25	-

3.4 FESEM of polymer-clay mixture

Figure 3 presents the interaction of polymer clay using FESEM. FESEM images indicate that the clay minerals in the sample are dominated by Kaolinite, Illite, and Montmorillonite (**Figure3**). **Figure 3(a)** exhibits the ragged appearance of the flat platelets that the Illite/Aam is detrital in origin [29]. The edge-face and face-face flocculation is common in clay aggregates and happens in the presence of freshwater. A similar effect in a different type of Illite clays had been observed in an earlier study by Pallatt et al [30, 31]. **Figure 3(b)** presents the FESEM of the Kaolinite/Aam composite. In the shale, there was no regularity in the surface with few ripples, indicating stacking of sheets of the material and crystalline-type order due to the existence of sodium phosphate hydrate and Montmorillonite. In a similar study by Rajat and Vikas (2015), they have polymerized a polyacrylamide/clay nanocomposite and using FESEM analysis have shown that by the existence of clay nanoparticles, the morphology of polyacrylamide has been changed[32]

. **Figure 2(c)** shows the FESEM of Montmorillonite/Aam composite. The image showed clustered surface particles, indicating that the presence of adsorbents increased the specific surface area of Montmorillonite and exposure of increasing metal ions that are in agreement with the findings of Feng et al., 2017 [33].

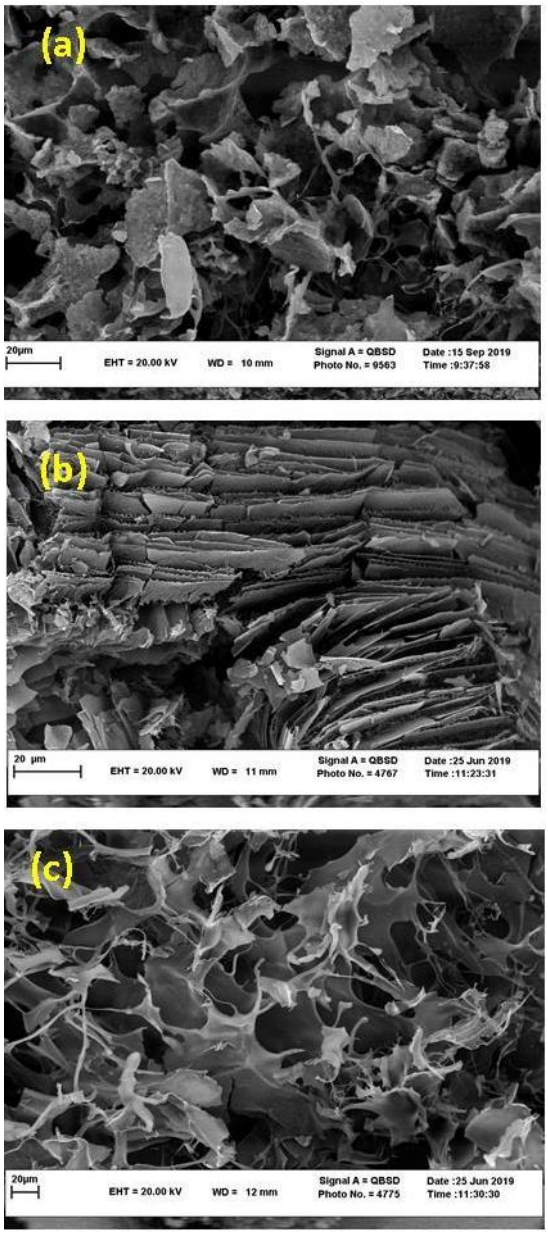

Figure 2. The FESEM images of (a) Illite/Aam b) Kaolinite/Aam, and c) Montmorillonite/Aam

3.5 Fourier transform infrared spectroscopy analysis (FTIR)

The synthesis of acrylamide- based hydrogels obtained from the FTIR spectra is shown in **Figure3**. According to the **f**igures, Kaolinite has triclinic layer structure and the combination of Kaolinite/Aam presents four (-OH) bands in the FTIR spectrum. The indicated peaks at 3652, and 3771 cm-1 are two of these that are assigned to vibrations of s-m and hydroxyl groups in kaoline. The peak 3657 cm-1 which is the third band is related to the vibrations resulting from inner hydroxyl groups in kaoline. The OH- bending area of Kaolinite indicates the surface OH groups near 836 cm-1and vibrations of the inner surface OH groups at 940 cm-1. The peaks around 755 and 703cm-1are associated with the surface hydroxyls. The bands stretching at 3657 cm-1 and in the region of 865-875 cm-1 are attributed to Fe bearing kaolinite. These stretching bands are extremely applied in the evaluation of the interface reactions and adsorption of this clay. The peaks in 700-950 are attributed to the structural OH^-bending mode in Montmorillonite/Aam and display a series of separate peaks that designates the cation composition in the octahedral sheets. The peak 2368 shows silicon function and the peak around 1650 cm-1 is due to amide-I of acrylamide units. C–N and C–H stretching bands appeared at 2929 cm-1, respectively, further confirming the presence of amide groups. Some of the characteristic peaks of acrylamide were red-shifted, the amide I band was shifted from 1661cm−1, in the cross-linked acrylamide, to 1650cm−1. The peaks at 1023 cm−1 in the FTIR spectrum are characteristic of skeletal vibration involving the stretching of C–O bonds in anhydrous glucose units. The spectrum showed a peak at 3421 cm–1 due to the stretching of –OH groups. The Illite/Aam curve shows the peak at 1023 cm–1 suggested –CH–O–CH– stretching. The characteristic peak at 1650 cm–1 was due to the amide-I band of the amide group of polyacrylamides (>C = O stretching vibration frequency). The peak at 1425 cm–1 suggested –CH bending of –CH2 group. This implies that the hydroxyl group of acrylamides is the preferred site for the reaction with the cross-linker and the grafting of acrylamide due to the lower steric hindrance of the primary hydroxyl group.

The results were approved with the recent study conducted in 2016 considered two sodium-based montmorillonite clays (Na-Mt) with one being modified with dodecyl trimethyl ammonium bromide (DTAB) and the other with cetyltrimethylammonium bromide (CTAB) for the removal of 4-chlorophenol (4-CP) and 2,4-di- chlorophenol (2,4-DCP). The spectral shows bands at several wavelengths, a sharp peak at the highest wavelength 3623 cm−1 resulted from the band due to hydroxyl group stretching vibrations [34].

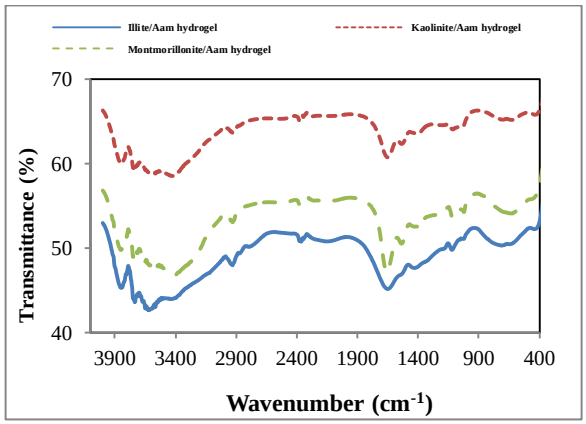

Figure 3. FTIR spectrum of clay-hydrogel composites

3.6 Swelling ratio study

Some physicochemical interactions between clays and water molecules are related to water dynamics. Kaolinite plays the role of an acceptable disintegrate due to its highly brittle and porous material that has a low swelling ability. Water penetration happens through pores via capillary forces. Electrostatic repulsion is a cause for increasing disintegration and that is because of the hydrated surfaces of kaolinite as overcame by permanent negative charges. Illite is a less swelling clay, almost the same as Kaolinite, and is adequate for a similar reduction rate for Kaolinite[35]. Based on the results, the properties of hydrogel were suggestively transformed by incorporating with different clays. The swelling capacity of three different hydrogels in distilled water is shown in **Figure 4**. By increasing the swelling ability of the hydrogels, the drug release and loading components within the hydrogel network are improved owing to the aggregate permeability of hydrogels that make them capable of releasing the entangled drugs more easily. It is obvious from **figure 4** that the swelling ratio of Montmorillonite/Aam is more than Kaolinite/Aam and Illite/Aam composites. The structure of the montmorillonite is effective in the swelling of the composite [36]. Montmorillonite is added as clay into a solution of monomer therefore Montmorillonite swells and the monomer enter the interlayer space of Montmorillonites. After that, a polymerization reaction can occur in situ in the interlayer space of Montmorillonite. The swelling stops when the distance between the layers reaches about 1 nm. The polymerization reaction is initiated by heat, in the presence of an initiator. The initiator was introduced into the interlayer space of Montmorillonite through cationic exchange [37] (**Figure 4**). In situ polymerization can directly produce bulky and long-chain polymers in the interlayer space of Montmorillonite. In addition, exothermic polymerization releases heat; the heat than could weaken the van der Waals force and electrostatic force between layers of Montmorillonite. As a result, Montmorillonite layers can be better exfoliated and dispersed in the polymer matrix. Goyanes et al. (2013) evaluated a coprecipitate of chitosan/ kaolin as disintegrate in the formulation of microcrystalline cellulose and hydrochlorothiazide (HCT) pellets. They demonstrated that these pellets led to complete and rapid disintegration in the dissolution medium, and do not significantly affect the dissolution of HTC, but increased the drug dissolution rate. Kristensen et al. (2002) studied the quality and efficiency of disintegrating pellets formulated with kaolin heavy and compared them to others formulated with bentonite. They confirmed that kaolin provides complete and fast disintegration to the pellet, while bentonite formulated pellet is erodible but not disintegrable [38, 39]. Recently, Devi et al. (2015) demonstrated a well-exfoliated O-Montmorillonite by prolonging the swelling of O-Montmorillonite in toluene by solution exfoliation [40, 41].

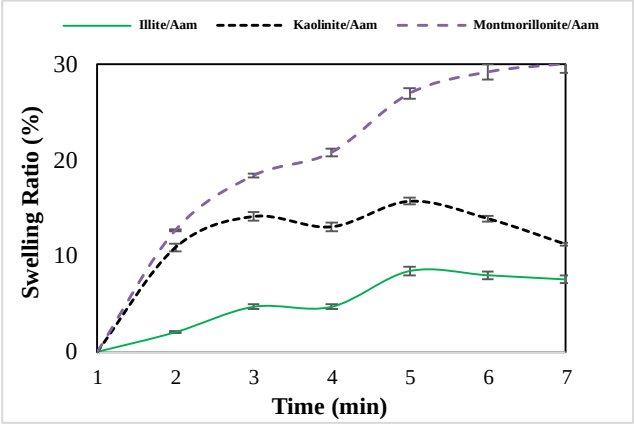

Figure 4: Swelling Behavior of Illite/Aam(a) Kalinite/Aam (b) and Montmorillonite/ Aam (c) Hydrogels

3.7 Rheological behavior

3.7.1 Frequency sweep

Electrostatic interactions are public in clay suspensions. Such interactions cause the extension in double layers and the double-layer repulsion determine the rheology, particularly with extended double layers and small particles [42]. **Figure 5 (a)** shows the mechanical spectra of clay-hydrogel at fixed stress (20 °C, 0.1 Pa), and the related rheological parameters are reported in **Table 3**. As can be seen in **Figure** 5 (a) at the applied frequency range, G' modulus of clay-hydrogels was larger than G", and there was no crossover. The results of frequency sweep confirm that due to the G" is always lower than G' in the applied frequency range, clay-hydrogels can be measured as a gel-type viscoelastic solid (**Figure 5 (a)**). The G' and G" value of the Illite/Aam G' (1260 ± 36.5 Pa) and (198.5 ± 6.6 Pa) was higher than the other mixtures. Montmorillonite/Aam G' performed the lowest G' (980 ± 23.4 Pa) and G" (153.5 ± 236 Pa) values, that approved the weakness of its molecular chain for the formation of the network. The tendance of higher molecular interaction in Kaolinite/ Aam and Illite/Aam G' hydrogel is caused in support of viscoelastic behavior (**Figure 5** (b)). As shown in **Table 3**, the results of the frequency sweep show that $\tan\delta$ clay-hydrogels were in the range of 0.16-0.20, which shows the weak gel structure of the biopolymer. The lowest $\tan\delta$ (0.16) was attributed to Illite/Aam that is related to the development of a stronger interlaced network. With increasing the frequency, the complex viscosity (η) of clay-hydrogels decreased and there was no flat region to observe in all the samples (**Figure 5**). An extensive range of colloidal behavior has been shown in clay mineral suspensions including viscoelasticity, thixotropy, and yield stress that depend on conditions of the aqueous environment, type of the applied clay, and the nature of the exchangeable cation [43]. For example, the rheological behavior of montmorillonite in water is extremely salt and pH-dependent [44]. In clay mineral suspensions, there is a huge interface separating the phases and this causes the rheology and stability to be strongly affected by non-hydrodynamic electrical double-layer forces. The stability of this type of suspension is dependent on the state of

accumulation of the particles and the rheology is both shear sensitive and chemistry [45, 46].

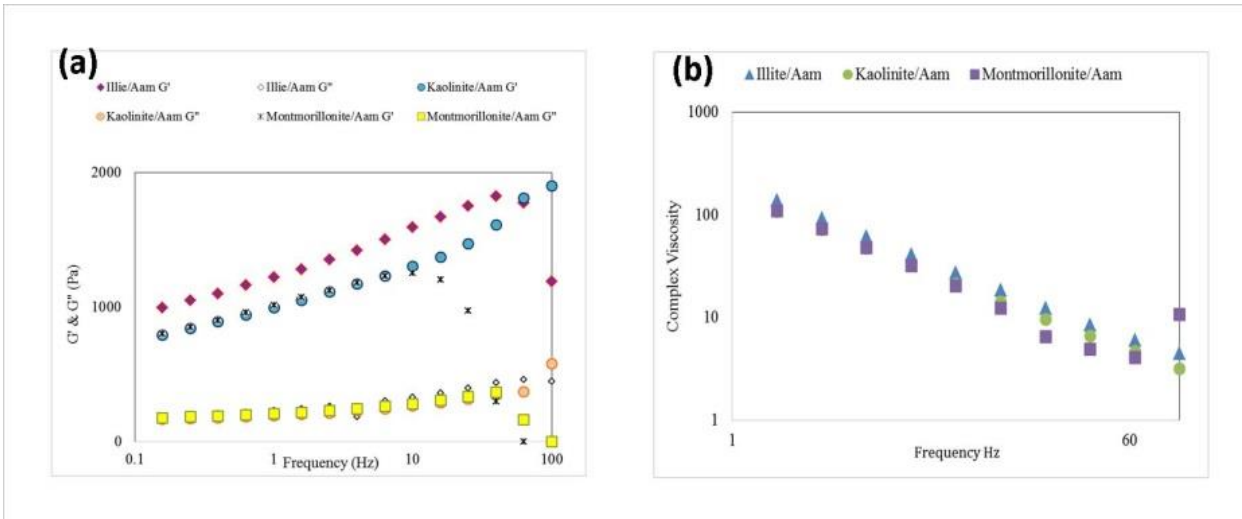

Figure 5. Mechanical spectra of clay-hydrogel examined by frequency sweep experiment (20℃, 0.1 Pa shear stress).

Table 3. Dynamic rheological factors of clay-hydrogels evaluated by frequency sweep experiment at 20℃, τ = 0.1 Pa, f = 1 Hz.

Sample	G' (Pa)	G"(Pa)	η (Pa. s)	Tan δ	Slope of $\eta - f$
Illite/Aam	1250	236.5	139.5	0.16	-6.3628x
Kaolinite/Aam	1021	198	109	0.18	-4.9579x
Montmorillonite/Aam	1040	213.5	111.5	0.20	-5.2757x

4. Conclusion

The findings of the study indicated that the incorporation of clays with polymer has been done properly based on the FTIR and FESEM results. The best clay to be applied in the hydrogel among these three types of clays is the montmorillonite, due to its highest swelling ratio rather than the other composites. The addition of clays changed the rheology behavior of the polymers. The existence of more molecular interaction in Kaolinite/ Aam, and Illite/Aam G' hydrogel resulted in support of viscoelastic behavior. In summary, swelling clays like montmorillonite interact strongly with the water and reduce its diffusive mobility at low temperatures compared to bulk water, whereas non-swelling clays either have a small effect (Illite) or even increase (Kaolinite) the diffusive mobility of the pore water. It is suggested to use the MXene as a new particle to the matrix of the clay/polymer and then study the different ratios of this novel particle. Studying the antimicrobial effect of this polymer can be effective for in-vitro studies.

References

1. Zhao Z, Fang R, Rong Q, Liu M. Bioinspired nanocomposite hydrogels with highly ordered structures. Advanced Materials. 2017;29(45):1703045.
2. Le X, Lu W, Zhang J, Chen T. Recent progress in biomimetic anisotropic hydrogel actuators. Advanced science. 2019;6(5):1801584.
3. Ludueña L, Morán J, Alvarez V. Biodegradable polymer/clay nanocomposites. Eco-friendly Polymer Nanocomposites. Springer; 2015. p. 109-35.
4. Nesrinne S, Djamel A. Synthesis, characterization and rheological behavior of pH sensitive poly (acrylamide-co-acrylic acid) hydrogels. Arabian Journal of Chemistry. 2017;10(4):539-47.
5. Onnainty R, Onida B, Páez P, Longhi M, Barresi A, Granero G. Targeted chitosan-based bionanocomposites for controlled oral mucosal delivery of chlorhexidine. International journal of pharmaceutics. 2016;509(1-2):408-18.
6. Vdović N, Jurina I, Škapin SD, Sondi I. The surface properties of clay minerals modified by intensive dry milling—revisited. Applied Clay Science. 2010;48(4):575-80.
7. Ozay O. Synthesis and swelling behavior of novel pH responsive hydrogels for environmental applications. Polymer-Plastics Technology and Engineering. 2014;53(2):130-40.
8. Shi Z, Gao X, Ullah MW, Li S, Wang Q, Yang G. Electroconductive natural polymer-based hydrogels. Biomaterials. 2016;111:40-54.
9. Gong X, Liu Y, Wang Y, Xie Z, Dong Q, Dong M, et al. Amino graphene oxide/dopamine modified aramid fibers: Preparation, epoxy nanocomposites and property analysis. Polymer. 2019;168:131-7.
10. Sabbagh F, Muhamad II. Acrylamide-based hydrogel drug delivery systems: release of acyclovir from MgO nanocomposite hydrogel. Journal of the Taiwan Institute of Chemical Engineers. 2017;72:182-93.
11. Jafarbeglou M, Abdouss M, Shoushtari AM, Jafarbeglou M. Clay nanocomposites as engineered drug delivery systems. RSC advances. 2016;6(55):50002-16.
12. Gao G, Du G, Sun Y, Fu J. Self-healable, tough, and ultrastretchable nanocomposite hydrogels based on reversible polyacrylamide/montmorillonite adsorption. ACS Applied Materials & Interfaces. 2015;7(8):5029-37.
13. Lin Z, Li P, Hou D, Kuang Y, Wang G. Aggregation mechanism of particles: Effect of Ca2+ and polyacrylamide on coagulation and flocculation of coal slime water containing illite. Minerals. 2017;7(2):30.
14. Brückner J, Thieme S, Böttger- Hiller F, Bauer I, Grossmann HT, Strubel P, et al. Carbon- based anodes for lithium sulfur full cells with high cycle stability. Advanced Functional Materials. 2014;24(9):1284-9.
15. Dong X, Duan X, Sun Z, Zhang X, Li C, Yang S, et al. Natural illite-based ultrafine cobalt oxide with abundant oxygen-vacancies for highly efficient Fenton-like catalysis. Applied Catalysis B: Environmental. 2020;261:118214.
16. Yang H, Tong D, Dong Y, Ren L, Fang K, Zhou C, et al. Kaolinite: A natural and stable catalyst for depolymerization of cellulose to reducing sugars in water. Applied Clay Science. 2020;188:105512.
17. Foroutan R, Mohammadi R, Adeleye AS, Farjadfard S, Esvandi Z, Arfaeinia H, et al. Efficient arsenic (V) removal from contaminated water using natural clay and clay composite adsorbents. Environmental Science and Pollution Research. 2019;26(29):29748-62.
18. Li P, Kim NH, Hui D, Rhee KY, Lee JH. Improved mechanical and swelling behavior of the composite hydrogels prepared by ionic monomer and acid-activated Laponite. Applied Clay Science. 2009;46(4):414-7.
19. Sabbagh F, Muhamad II. Physical and chemical characterisation of acrylamide-based hydrogels, Aam, Aam/NaCMC and Aam/NaCMC/MgO. Journal of Inorganic and Organometallic Polymers and Materials. 2017;27(5):1439-49.
20. Sabbagh F, Khatir NM, Karim AK, Omidvar A, Nazari Z, Jaberi R. Mechanical Properties and Swelling Behav-ior of Acrylamide Hydrogels using Mont-morillonite and Kaolinite as Clays. Journal of Environmental Treatment Techniques. 2019;7(2):211-9.
21. Sabbagh F, Muhamad II, Nazari Z, Mobini P, Khatir NM. Investigation of acyclovir-loaded, acrylamide-based hydrogels for potential use as vaginal ring. Materials Today Communications. 2018;16:274-80.
22. Sachan A, Penumadu D. Identification of microfabric of kaolinite clay mineral using X-ray diffraction technique. Geotechnical and Geological Engineering. 2007;25(6):603.
23. Brindley G. An X-ray method for studying orientation of micaceous minerals in shales, clays, and similar materials. MinM. 1953;30(220):71-8.
24. Young R, Hewat A. Verification of the triclinic crystal structure of kaolinite. Clays and Clay Minerals. 1988;36(3):225-32.
25. Kampeerapappun P, Aht-ong D, Pentrakoon D, Srikulkit K. Preparation of cassava starch/montmorillonite composite film. Carbohydrate Polymers. 2007;67(2):155-63.
26. Sabbagh F, Kiarostami K, Mahmoudi Khatir N, Rezania S, Muhamad II. Green Synthesis of Mg0. 99 Zn0. 01O Nanoparticles for the Fabrication of κ-Carrageenan/NaCMC Hydrogel in order to Deliver Catechin. Polymers. 2020;12(4):861.
27. Marsh A, Heath A, Patureau P, Evernden M, Walker P. Alkali activation behaviour of un-calcined montmorillonite and illite clay minerals. Applied Clay Science. 2018;166:250-61.
28. Gailhanou H, Van Miltenburg J, Rogez J, Olives J, Amouric M, Gaucher EC, et al. Thermodynamic properties of anhydrous smectite MX-80, illite IMt-2 and mixed-layer illite–smectite ISCz-1 as determined by calorimetric methods. Part I: Heat capacities, heat contents and entropies. Geochimica et Cosmochimica Acta. 2007;71(22):5463-73.
29. Huggett JM. Formation of authigenic illite in palaeocene mudrocks from the central North Sea: A study by high resolution electron microscopy. Clays and clay minerals. 1995;43(6):682-92.
30. Pallatt N, Wilson J, McHardy B. The relationship between permeability and the morphology of diagenetic illite in reservoir rocks. Journal of Petroleum Technology. 1984;36(12):2,225-2,7.
31. Bakar WZW, Saaid IM, Ahmad MR, Jarni HH, Mahat SQA. An Investigation on the Effect of Solvent and Heat to Clay Minerals in Shaly Sandstone. Indonesian Journal of Chemistry.
32. Jain R, Mahto V, Sharma V. Evaluation of polyacrylamide-grafted-polyethylene glycol/silica nanocomposite as potential additive in water based drilling mud for reactive shale formation. Journal of Natural Gas Science and Engineering. 2015;26:526-37.
33. Feng Y-l, Yu L-j, Cao R-w. Adsorption of Copper ions by Montmorillonite/Sodium Humate/N-Isopropyl Acrylamide composite. BULGARIAN CHEMICAL COMMUNICATIONS. 2017;49(3):685-9.
34. Puchana-Rosero M, Adebayo MA, Lima EC, Machado FM, Thue PS, Vaghetti JC, et al. Microwave-assisted activated carbon obtained from the sludge of tannery-treatment effluent plant for removal of leather dyes. Colloids and Surfaces A: Physicochemical and Engineering Aspects. 2016;504:105-15.
35. Awad ME, López-Galindo A, Setti M, El-Rahmany MM, Iborra CV. Kaolinite in pharmaceutics and biomedicine. International Journal of Pharmaceutics. 2017;533(1):34-48.
36. Sánchez FG, Van Loon LR, Gimmi T, Jakob A, Glaus MA, Diamond LW. Self-diffusion of water and its dependence on temperature and ionic strength in highly compacted montmorillonite, illite and kaolinite. Applied Geochemistry. 2008;23(12):3840-51.
37. Roghani- Mamaqani H, Haddadi- Asl V, Najafi M, Salami-Kalajahi M. Preparation of nanoclay- dispersed polystyrene nanofibers via atom transfer radical polymerization and electrospinning. Journal of applied polymer science. 2011;120(3):1431-8.
38. Zhu TT, Zhou CH, Kabwe FB, Wu QQ, Li CS, Zhang JR. Exfoliation of montmorillonite and related properties of clay/polymer nanocomposites. Applied Clay Science. 2019;169:48-66.
39. Goyanes A, Souto C, Martínez-Pacheco R. Chitosan–kaolin coprecipitate as disintegrant in microcrystalline cellulose-based pellets elaborated by extrusion–spheronization. Pharmaceutical development and technology. 2013;18(1):137-45.
40. Kristensen J, Schæfer T, Kleinebudde P. Development of fast-disintegrating pellets in a rotary processor. Drug development and industrial pharmacy. 2002;28(10):1201-12.
41. Devi KU, Ponnamma D, Causin V, Maria HJ, Thomas S. Enhanced morphology and mechanical characteristics of clay/styrene butadiene rubber nanocomposites. Applied clay science. 2015;114:568-76.

42. Tadros TF. Rheology of dispersions: principles and applications. John Wiley & Sons; 2011.
43. Paineau E, Bihannic I, Baravian C, Philippe A-M, Davidson P, Levitz P, et al. Aqueous suspensions of natural swelling clay minerals. 1. Structure and electrostatic interactions. Langmuir. 2011;27(9):5562-73.
44. Tombacz E, Szekeres M. Colloidal behavior of aqueous montmorillonite suspensions: the specific role of pH in the presence of indifferent electrolytes. Applied clay science. 2004;27(1-2):75-94.
45. Cruz N, Peng Y. Rheology measurements for flotation slurries with high clay contents–a critical review. Minerals Engineering. 2016;98:137-50.
46. Sabbagh F, Kiarostami K, Khatir NM, Rezania S, Muhamad II, Hosseini F. Effect of zinc content on structural, functional, morphological, and thermal properties of kappa-carrageenan/NaCMC nanocomposites. Polymer Testing. 2021;93:106922.